THE JOURNAL OF PHYSICAL CHEMISTRY B

Article

pubs.acs.org/JPCB

Photoaddition of Two Guanine Bases to Single Ru-TAP Complexes. Computational Studies and Ultrafast Spectroscopies to Elucidate the pH Dependence of Primary Processes

Lionel Marcélis,[§,⊥] Mateusz Rebarz,[†,⊥] Vincent Lemaur,[‡] Eduard Fron,[@] Julien De Winter,[∥] Cécile Moucheron,[§] Pascal Gerbaux,[∥] David Beljonne,[‡] Michel Sliwa,*[,†] and Andrée Kirsch-De Mesmaeker*[,§]

[§]Chimie Organique et Photochimie, Université Libre de Bruxelles, CP 160/08, 50 Avenue Franklin Roosevelt, B-1050 Brussels, Belgium

[†]Laboratoire de Spectrochimie Infrarouge et Raman UMR 8516, CNRS-Université Lille 1 Sciences et Technologies, 59655 Villeneuve d'Ascq Cedex, France

[‡]Laboratory for Chemistry of Novel Materials, UMons, 20 Place du Parc, B-7000 Mons, Belgium

[@]Molecular Imaging and Photonics, KULeuven, Celestijnenlaan 200f, B-3001 Leuven, Belgium

[∥]Organic Synthesis and Mass Spectrometry Laboratory, University of Mons, UMons, 23 Place du Parc, B-7000 Mons, Belgium

Supporting Information

ABSTRACT: The covalent photoadduct (**PA**) between $[Ru(TAP)_3]^{2+}$ (TAP = 1,4,5,8-tetraazaphenanthrene) and guanosine monophosphate (GMP) opened the way to interesting photobiological applications. In this context, the **PA**'s capability upon illumination to give rise to the addition of a second guanine base is especially interesting. The origins of these intriguing properties are for the first time thoroughly investigated by an experimental and theoretical approach. The **PA**'s spectroscopic and redox data combined with TDDFT results corroborated with resonance Raman data show that the properties of this **PA** (pK_a around 7) depend on the solution pH. Theoretical results indicate that the acid form **PA.H**$^+$ when excited should relax to MLCT (metal-to-ligand charge transfer) excited states, in contrast to the basic form **PA** whose excited state should have LLCT/ILCT (ligand-to-ligand charge transfer/intra ligand charge transfer) characteristics. Ultrafast excitation of **PA.H**$^+$ at pH 5.9 produces continuous dynamic processes in a few hundred picoseconds involving coupled proton−electron transfers responsible for luminescence quenching. Long-lived species of a few microseconds capable of reacting with GMP are produced at that pH, in agreement with the formation of covalent addition of a second GMP to **PA**, as shown by mass spectrometry results. In contrast, at pH 8 (mainly nonprotonated **PA**), other ultrafast transient species are detected and no GMP biadduct is formed in the presence of GMP. This pH dependence of photoreaction can be rationalized with the different nature of the excited states, thus at pH 8, unreactive LLCT/ILCT states and at pH 5.9 reactive MLCT states.

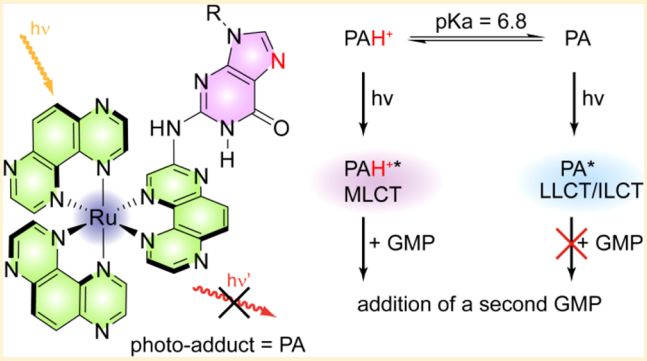

1. INTRODUCTION

Polypyridyl ruthenium complexes have been the focus of numerous studies dealing with their photophysical and photochemical properties for many years. Thus, since the first studies of $[Ru(bpy)_3]^{2+}$ (bpy = 2,2′-bipyridine),[1−3] numerous new ligands generating novel Ru^{II} complexes have been prepared and used in various research fields such as solar energy conversion,[4] water splitting,[5,6] molecular machines,[7,8] and in biological applications.[9−12] Among the various ligands that have been developed not only for complexation with the Ru ion but also with other transition metal ions, the TAP ligand (TAP = 1,4,5,8-tetraazaphenanthrene) and derivatives have been the subject of increasing interest in the literature during these last few years.[13−19] In spite of the TAP similarity with the extensively used phen ligand (phen = 1,10-phenanthroline), the two supplementary N atoms of TAP (Figure 1) are the origin of its attractive properties in coordination chemistry as exemplified also in the present work. Due to its enhanced π-deficiency, the TAP confers to the corresponding complexes an increased photo-oxidation power as compared to phen-equivalent complexes. Therefore, in the presence of a reducing agent this results in a photoinduced electron transfer (ET).

Received: January 8, 2015
Revised: March 6, 2015
Published: March 6, 2015

DOI: 10.1021/acs.jpcb.5b00197
J. Phys. Chem. B 2015, 119, 4488−4500

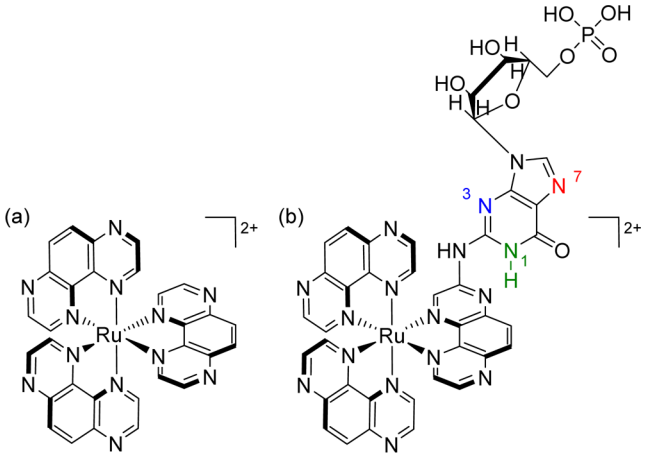

Figure 1. Structure of (a) $[Ru(TAP)_3]^{2+}$ and (b) its photoadduct with GMP, **PA** = $[Ru(TAP)_2(TAP(GMP))]^{2+}$. The GMP motif is tilted to form a hydrogen bond between the guanine unit (NH position 1) and the nitrogen of the TAP(G) ligand (see below DFT calculations).

More particularly in the area of biology, the Ru compounds based on this TAP ligand are of peculiar interest.[11,13−15,17,19] In the presence of DNA,[20,21] the ET process takes place between the DNA guanine (G) bases and the complex under irradiation. This photoinduced ET produces radical species that either give rise to the back electron transfer (BET) process with regeneration of the starting material or after several reaction steps lead to a final photoproduct. This latter has been isolated, and its structure has been determined.[22,23] It corresponds to a covalent adduct of one G base or guanosine monophosphate (GMP) to the complex such as $[Ru(TAP)_3]^{2+}$ (Figure 1a). During several years, efforts have been focused on the use and applications of this light-triggered reaction to target G bases of a specific DNA sequence and, in this way, damage DNA at specific sites.[20,24]

It has also been shown that when such a photoadduct is formed at a G base of an oligonucleotide, further illumination of this Ru-damaged oligonucleotide in the presence of its complementary strand containing another G unit induces an irreversible photo-cross-linking between the two strands.[25] This finding is extremely interesting since, thanks to these photoprocesses, two complementary G-containing oligonucleotides can irreversibly be linked together via a single Ru-TAP complex.[11,25,26] AFM studies have also shown that such photo-cross-linkings can even occur between G bases belonging to different portions of a DNA plasmid.[11,26] These discoveries have prompted us to try to understand the origin of such cross-linking processes.

The mechanism of formation under illumination of the monoadduct like the one in Figure 1b seems to be well-understood presently. It involves a proton coupled electron transfer (PCET) process from a DNA's G base to the ^{3}MLCT (metal to ligand charge transfer) state of the complex.[27] This process is of course accompanied by a luminescence quenching of the excited Ru-TAP complex. In order to obtain a photo-cross-linking between two DNA strands, it could be imagined that once the monoadduct is formed, its further irradiation would give rise to another PCET from another G base belonging to the other strand. However, this explanation could not easily be compatible from the fact that when the monoadduct is isolated, it is not emissive, suggesting that the excited state lifetime is shortened by a quenching process. The origin of this photo-cross-linking is thus rather intriguing. Moreover, since this photoreactivity is characteristic of TAP ligands, maybe it might be extended to complexes with other metal ions. The investigation of the origin of this photoinduced reactivity is thus important.

The goal of this work is, in a first step, to demonstrate the formation of G biphoto-adduct, no longer by the occurrence of oligonucleotides or DNA strands cross-linkings as explained above but by detection of GMP biadducts upon illumination in the presence of GMP. In a second step, we want to investigate the behavior of the isolated monophoto-adduct (Figure 1b), in view of understanding the origin of its nonemissive property and, in spite of this, its photoreaction with GMP to form biphoto-adduct. In this study, we have thus examined the properties of the isolated monophoto-adduct **PA** (Figure 1b) by a combination of experimental and theoretical approaches. After examination of its spectroscopic characteristics and the required conditions to obtain a biadduct from **PA** in the presence of GMP, the rational interpretation of the spectral and redox data needed a computer modeling study, corroborated with resonance Raman data. Moreover, the excited state dynamic processes from the femto- to the microsecond time domain, in comparison with that of the reference $[Ru(TAP)_3]^{2+}$ complex, highlight not only the origin of the absence of luminescence of **PA** but lead also to rational explanations of the pH conditions necessary to form the biadduct.

2. EXPERIMENTAL SECTION

2.1. Preparation of Photoadduct. In a triple wall Pyrex photoreactor, $[Ru(TAP)_3]^{2+}$ (100 mL, 5.6×10^{-5} M) in the presence of a mixture of Na_2GMP (2×10^{-3} M) and H_2GMP (2×10^{-3} M) (pH 6) was illuminated for 7 h, under an argon atmosphere with continuous stirring, using a 250 W xenon lamp (Phillips). The photoreactor was maintained at room temperature by a continuous water flow around the lamp. The photoreaction was followed by UV−visible absorption spectroscopy and analytical HPLC. The irradiation was stopped after 7 h. The $[Ru(TAP)_3]^{2+}$ complex was synthesized following previous reports.[28] All chemicals and solvents used were of spectro-chemical grade. Water was obtained by a Milli-Q system.

2.2. HPLC. HPLC analysis and purification were realized using a modular Waters HPLC system based on a quaternary 2535 pump, a 2707 autosampler, a 2998 PDA detector, a 2475 fluorimeter, and a WFC-III fraction collector. The whole system was controlled by Waters (Empower 3). The elutions were performed on an Atlantis T3 column with an isocratic water/acetonitrile 90−10 eluent containing 0.1% of TFA. Semipreparative HPLC purifications were also performed using the same elution mixture.

2.3. Steady-State Spectroscopy. The emission spectra were recorded with a Shimadzu RF-5301PC and the absorption spectra with a PerkinElmer Lambda 40 UV−vis spectrophotometer. The steady-state illuminations in the presence of GMP were performed with a Thermo Oriel xenon lamp (500 W). Water was allowed to circulate through an IR filter and a 0.2 M $NaNO_2$ solution was used to cut off the UV.

2.4. Voltammetry. Differential pulse voltammetry was carried out on a gold working electrode (approximate area = 3 mm^2), in dried acetonitrile with tetrabutylammonium hexafluorophosphate (0.1 mol L^{-1}) as the supporting electrolyte. The potential of the working electrode was controlled by an Autolab PGSTAT 100 (Eco Chemie B.V., Utrecht, The

DOI: 10.1021/acs.jpcb.5b00197
J. Phys. Chem. B 2015, 119, 4488−4500

Netherlands) potentiostat through a PC interface with a scan rate of 100 mV s^{-1} between −2 and +2 V versus Ag/AgCl. The counter electrode was a gold disk, and the reference electrode a Leakless Miniature ET072 (EDAQ). All measurements were performed in a single compartment cell and under argon.

2.5. Mass Spectrometry. MALDI mass spectra were recorded using a Waters QToF Premier mass spectrometer equipped with a nitrogen laser, operating at 337 nm with a maximum output of 500 J m^{-2} delivered to the sample in 4 ns pulses at 20 Hz repeating rate. Time-of-flight mass analyses were performed in the reflectron mode at a resolution of about 10000 at m/z 500. The matrix, α-cyano-4-hydroxycinnamic acid (CHCA), was prepared in water (20 mg mL^{-1}). The matrix solution (1 μL) was applied to a stainless steel target and air-dried. Samples were dissolved in water (1 mg mL^{-1}). One microliter aliquots of these solutions were applied to the target area already bearing the matrix crystals and then air-dried. For the recording of the single-stage MALDI-MS spectra, the quadrupole (rf-only mode) was set to pass ions from m/z 50 to 1500, and all ions were transmitted into the pusher region of the time-of-flight analyzer where they were mass analyzed with 1 s integration time. Data were acquired in continuum mode until acceptable averaged data were obtained.

2.6. Raman and Resonance Raman Spectroscopy. The sample was placed on an inverted microscope (TiU, Nikon). The Raman signals were collected and sent to a spectrometer (iHR 320, Horiba) equipped with a cooled electron multiplying charge-coupled device (CCD) camera (Newton 920, Andor). The excitation light was delivered by cw diode and Ar lasers and the power density used was ca. 1−10 kW cm^{-2}. Each spectrum was averaged 100 times, while the integration time was set to 0.5 s.

2.7. Fluorescence Decays. The fluorescence decay time constants were determined by TCSPC measurements, and the setup has been described in detail previously.[29] A time-correlated Single Photon Counting PC module (SPC 830, Becker & Hickl) was used to obtain the fluorescence decay histogram in 4096 channels. The decays were recorded with 10^4 counts in the peak channel, in time windows of 20 ns corresponding to 4.9 ps/channel and analyzed globally with time-resolved fluorescence analysis (TRFA) software. The full width at half-maximum (fwhm) of the IRF was typically on the order of 40 ps. The quality of the fits was judged by the fit parameters χ^2 (<1.2), Z_χ^2 (<3), and the Durbin Watson parameter (1.8 < DW < 2.2), as well as by the visual inspection of the residuals and autocorrelation function. All measurements were performed in cuvettes with an optical path length of 1 cm at an optical density of ca. 0.1 at the excitation wavelength of 395 nm.

2.8. Ultrafast Transient Absorption Spectroscopy, Picosecond Time-Domain. The ultrafast transient absorption experiments were carried out using an apparatus described elsewhere.[30] Briefly, 1 kHz Ti:sapphire laser system delivered 100 fs (0.8 mJ) pulses at 800 nm. The excitation pulses were obtained from an OPA (Palitra, Excel Continuum). Pump pulse energy at the sample was about 3 μJ with a diameter of about 0.5 mm (1.5 mJ/cm^2). The white light continuum probe beam was generated by focusing the fundamental beam in a 1 mm CaF_2 rotating plate. The pump−probe polarization configuration was set at the magic angle (54.7°), and the probe pulse was delayed in time relative to the pump pulse using an optical delay line. The white light continuum was split into a probe beam (with pump) and a reference beam (without pump). The transmitted light of the probe and reference beam was recorded on two different channels of a multichannel spectrograph equipped with a CCD camera (Princeton Instrument), and the transient spectra were computed. The samples were placed in a quartz cell with path length of 1 mm, and the studied materials were diluted to get a concentration corresponding to optical density of about 0.8 at the pump wavelength. Stability of the sample was checked after each experiment. The instrumental response function of about 200 fs was estimated measuring the stimulated Raman amplification signal from the solvent. All experimental data were corrected from the group velocity dispersion, and global decay analysis (using Igor Pro 6.20) was applied to get time constants for the transients.

2.9. Transient Absorption Spectroscopy, Nano- and Microsecond Time-Domain. Nanosecond laser flash photolysis setup was described in detail elsewhere.[31] Briefly, the excitation pulses (fwhm ∼4 ns, 1 mJ, 0.5 Hz) were provided by a 10-Hz Nd:YAG laser coupled to an OPO. The probe light was provided by a pulsed Xe lamp. The transmitted light was dispersed by a monochromator and analyzed with a photomultiplier coupled to a digital oscilloscope. The recorded traces were averaged for several pulses and repeated for different wavelengths to reconstruct the spectra afterward. The deconvolution procedure of the individual decays with an experimentally measured instrument response function for single wavelengths analyses of the transient absorption data were performed using Igor Pro 6.20. Samples were contained in a quartz cell (10 × 10 mm) at an adjusted concentration corresponding to optical density about 0.5 at the pump excitation wavelength. The solutions were deoxygenated by bubbling argon for at least 20 min before the measurements. The same setup was used to record the luminescence decays in nanosecond and microsecond timescales.

2.10. Quantum-Chemical Calculations. The ground-state geometry of the Ru^{II} complexes has been optimized at the density functional theory (DFT) level. The chosen exchange correlation functional is the widely used B3LYP functional in view of its good compromise between accuracy and computational cost; the basis set for the description of the electrons of nonmetallic atoms is 6-31G**, while the LANL2DZ basis set has been used for the ruthenium center. The energies and nature of the electronic orbitals as well as the characterization and nature of the excited states involved in the absorption spectra rely on time-dependent density functional theory (TD-DFT) calculations performed on the basis of the optimized ground-state geometries, using the same functional and basis set. The PCM (polarizable continuum model) scheme has been coupled to all DFT and TD-DFT calculations to account for solvent (water) effects. Within this model, the solute is embedded in a shape-adapted cavity surrounded by the solvent implicitly described by a dielectric continuum, which is characterized by a dielectric constant (ε = 78.4 for water). All the calculations were performed with Gaussian 09.[32] The red/blue [yellow/green] isosurfaces of Figure S8 (panels d−f) of the Supporting Information have been generated by the Jmol program[33] by combining for each atom the LCAO coefficients in all the occupied [unoccupied] molecular orbitals involved in the TD-DFT description of the excited state and their weights in the wave functions.[34]

3. RESULTS AND DISCUSSION

3.1.a. Photosynthesis, Isolation, and Spectroscopic Characterization of the Monophoto-Adduct (PA). The

DOI: 10.1021/acs.jpcb.5b00197
J. Phys. Chem. B 2015, 119, 4488−4500

photoadduct $[Ru(TAP)_2(TAP(GMP))]^{2+}$ (Figure 1b) (**PA**) was prepared by photosynthesis from $[Ru(TAP)_3]^{2+}$ with GMP. A pH lower than 7 was necessary because at a higher pH **PA** was not formed. Therefore, a pH of 5.9 was chosen for the present **PA** photosynthesis. Moreover, an argon atmosphere was required to avoid the presence of secondary oxidized products.[35] The targeted $[Ru(TAP)_2(TAP(GMP))]^{2+}$ was separated with difficulty from the starting complex $[Ru(TAP)_3]^{2+}$ by successive cation-exchange column chromatographies. Semipreparative HPLC purifications were also needed to remove the excess of GMP and the starting complex from the desired **PA**.

Once isolated and purified, the absorption and emission spectra of **PA** were recorded in a Tris buffer medium. As previously observed, no emission or only an extremely weak emission, depending on the prepared sample, could be detected (Figure S1 of the Supporting Information).[36] Unexpectedly, the absorption spectrum of **PA** is pH sensitive (Figure 2a). At pH

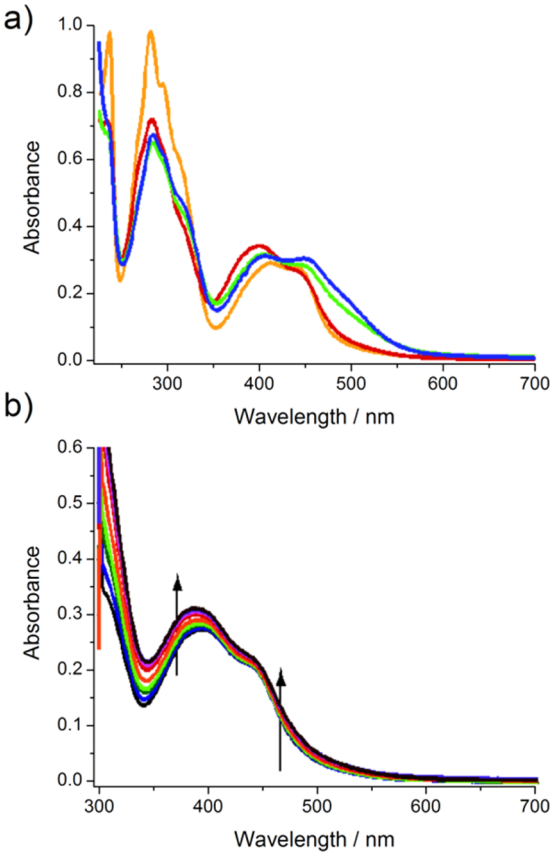

Figure 2. (a) Absorption spectra of $[Ru(TAP)_3]^{2+}$ (orange) and **PA** or **PA.H**$^+$ at pH 5.9 (red), 7.4 (green), and 8.0 (blue) in H_2O (0.1 M Tris buffer); the ratio of absorbance at 500 nm versus 450 nm corresponds to 0.23, 0.50, and 0.55 at pH 5.9, 7.4, and 8.0, respectively. (b) Change of the absorption spectra of **PA.H**$^+$ irradiated in the presence of GMP 10 mM at pH 5.9 during 4 h under argon.

lower than 5.9, the **PA** absorption in the visible range exhibits a maximum which is slightly shifted to the blue relative to the absorption maximum of $[Ru(TAP)_3]^{2+}$, in agreement with the spectroscopic signature reported for the formation of **PA** on DNA.[23] However, at pH 8, a shoulder appears around 490−500 nm. This pH dependence of the **PA** absorption indicates the presence of an acid−base reaction. The evolution of the absorbance at 370 and 490 nm allows the determination of a pK_a value around 6.8 (Figure S2 of the Supporting Information). This pK_a cannot correspond to the phosphate group[37] or the protonation of a TAP ligand, which occurs only at much lower pH values.[38] Therefore, it should correspond to protonation of the **PA's** guanine group. Thus, at pH around 6 and lower, mainly the protonated G group of **PA** should exist (**PA.H**$^+$), and at pH 8, mainly the basic form **PA** should be present.[39] It was also tested that neither protonated nor nonprotonated **PA** was luminescent.

3.1.b. Evidence for Formation of a Biadduct under Illumination. The isolated **PA** was also illuminated under steady state conditions at pHs 5.9 and 8 in the presence of 10 mM GMP in order to detect the formation of biadduct from the monoadduct **PA**. As shown in Figure 2b at pH 5.9, there is a hyperchromic effect of the absorption spectrum as a function of the illumination time. In contrast, there is no transformation at pH 8 (Figure S3 of the Supporting Information). This is consistent with the experimental condition needed for the photosynthesis of monoadduct **PA** from the starting complex $[Ru(TAP)_3]^{2+}$. In order to confirm that a biadduct is potentially obtained, MALDI mass spectrometry experiments have been performed on the solution illuminated at pH 5.9 and 8. At pH 5.9, a signal at m/z 1370 confirms the presence of a biadduct (Figure S4a of the Supporting Information), and interestingly, in the spectrum at pH 8 (Figure S4b of the Supporting Information), no signal around m/z 1370 mass range is observed. To get more information on the structure of the biadduct, tandem mass spectrometry analyses have then been performed on the biadduct ions (m/z 1370) (Figure 3) and the initial **PA** (m/z 1009) (Figure S4c of the Supporting Information) for comparison purposes.

It has to be remembered that, as described previously with a MALDI source,[21] the ionized products involve at least two competitive processes with production of two different singly charged species: (i) a one-electron capture by the doubly charged analyte, which generates in the present case, a radical cation at m/z 1009 for **PA**, and m/z 1370 for the biadduct or (ii) a one proton loss from a phosphate moiety, which gives rise to a cation at m/z 1008 for **PA** and m/z 1369 for the biadduct (Figure 3 and Figure S4c of the Supporting Information). It is impossible to isolate the cationic from the radical cationic counterparts prior to the MS/MS experiments. Therefore, the spectrum in Figure 3 exhibits the fragmentations for the biadduct singly charged species (at m/z 1369−1370). In that case and by comparison with fragmentation of **PA** (Figure S4c of the Supporting Information), the presence of two consecutive ribose phosphate residue losses, generating m/z 1157−1158 and 945−946 ions, confirms indeed the presence of two GMP residues. Interestingly, a 543 u loss, affording m/z 826 ions, is easily ascribed to the direct elimination of one TAP(GMP) ligand. This observation leads thus to the conclusion that two GMP moieties are present on two different TAP ligands in the biadduct. However, we have also to note that a more detailed analysis of this MALDI tandem mass spectrum (Figure S5 of the Supporting Information) recorded for the biadduct confirms the presence of another biadduct isomer, bearing in that case the two GMP groups on the same TAP ligand.

In conclusion, for the first time it is demonstrated by single stage MALDI mass spectrometry and tandem mass spectrometry that it is possible to photosynthesize a biadduct using **PA** as reagent in the presence of GMP.

DOI: 10.1021/acs.jpcb.5b00197
J. Phys. Chem. B 2015, 119, 4488−4500

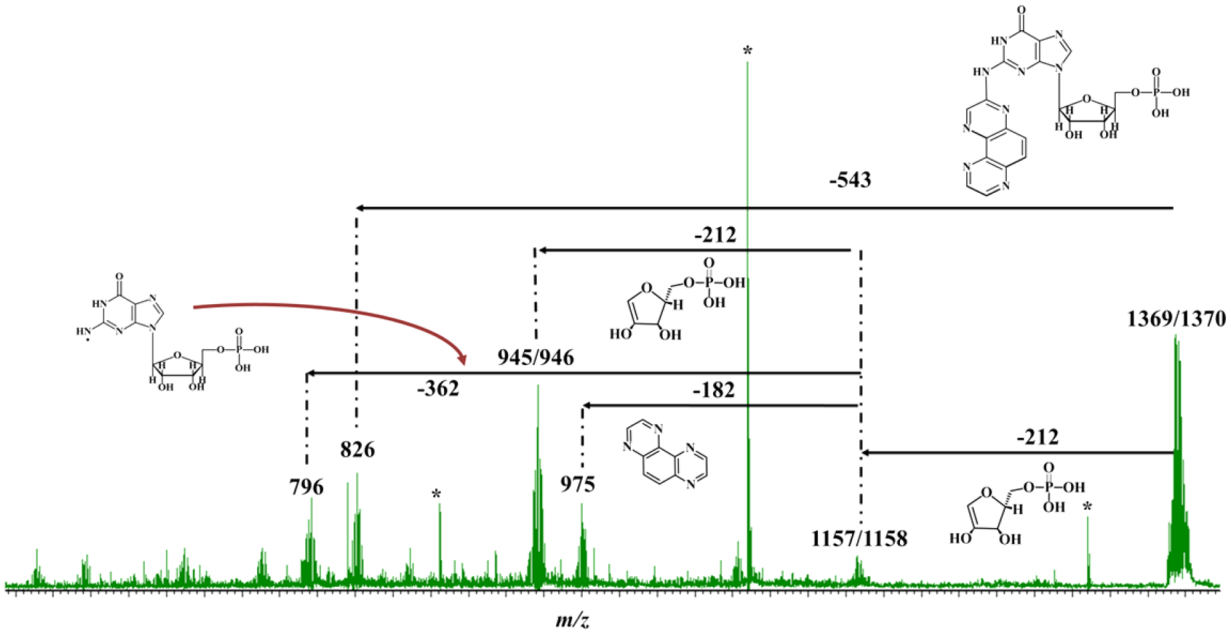

Figure 3. MALDI tandem mass spectrum recorded for biphoto-adduct (m/z 1369−1370). Signals marked with a star are attributed to the fragmentation of isobaric contaminations.

Moreover, as previously described for the photosynthesis of **PA** from $[Ru(TAP)_3]^{2+}$, the pH has to be lower than 7 for the photoreaction of **PA** to proceed efficiently. It is also shown that at least two types of biphoto-adducts are formed, one with one GMP on two different TAP ligands and one with the two GMP on the same TAP ligand. The following study and discussions deal only with the monoadduct **PA**.

3.2. Electrochemistry of PA. In view of further characterizing the ground state properties of the **PA**, electrochemical measurements were performed by cyclic voltammetry (CV) in MeCN. Due to the rather poor solubility of **PA** in organic solvents and the small amount at our disposal, the CV curves were recorded with a miniaturized electrochemical cell (see Experimental Section) by differential pulsed voltammetry (Figure S6 of the Supporting Information). As the **PA** was isolated from a mixture of water and MeCN, it is difficult to know at this stage which **PA** species is present after dissolution in MeCN (**PA**, **PA.H**$^+$, or both). The potential values are gathered in Table 1 together with those of the parent $[Ru(TAP)_3]^{2+}$ complex, measured in the same conditions.

Table 1. Oxidation and Reduction Potentials of the Photo-Adduct[a]

complex	E_{ox} (V vs SCE)	E_{red} (V vs SCE)
$[Ru(TAP)_3]^{2+}$	+2.02	−0.75; −0.88; −1.10
photoadduct	+1.96; +2.16	−0.69; −0.96; −1.14

[a]Measurements in dried MeCN by differential pulsed voltammetry (0.1 M $TBAPF_6$ as supporting electrolyte; gold working electrode and gold counter-electrode; Ag/AgCl electrode as reference; E^0Ag/AgCl = −0.019 V vs SCE).

Interestingly, two oxidation waves can clearly be detected (Figure S6a of the Supporting Information), the first wave appears at a slightly less positive potential than the one for the oxidation of the Ru center in $[Ru(TAP)_3]^{2+}$. This contrasts with the normal single Ru^{2+}/Ru^{3+} wave observed for most mononuclear Ru^{II} complexes. The presence of these two waves for **PA** indicates that in addition to the Ru^{II} center, another species is also oxidized. It is obvious that the only difference between $[Ru(TAP)_3]^{2+}$ and **PA** is the presence of the G substituent. Therefore, the supplementary anodic wave for **PA** can only be attributed to the additional guanine base moiety. It is difficult at this stage to assign the first oxidation to the Ru or the guanine base. In reduction, **PA** exhibits three waves, the first one at a potential slightly less negative than that for $[Ru(TAP)_3]^{2+}$.

In order to determine the origins of the differences in the electrochemical data for **PA** and $[Ru(TAP)_3]^{2+}$, as well as for the spectroscopic data, (TD)DFT calculations have been performed.

3.3. (TD)DFT Calculations and Comparison with the Spectroscopic and Electrochemical Data. DFT calculations provide insightful information on **PA** such as the nature of the electronic transitions associated with both the basic and acid forms, the localization and energy of the most frontier molecular orbitals, as well as the most favorable sites of protonation and hence the structure of the resulting **PA.H**$^+$.

First, the relative energies of different protonated **PA** species were calculated in order to determine the most stable structure and thus the most probable protonation site. For simplifying the calculations, the sugar−phosphate group has been omitted, as it is very likely that it would not influence the protonation and electronic properties of **PA**. The results show that a protonation at position 7 of the guanine unit (Figure S7 of the Supporting Information) is by far more favorable by 11.1 kcal/mol than a protonation at position 3. This protonation pattern was the same as that calculated for isolated guanine in water.[40] When flipping by 180°, the protonated guanine moiety of the most stable conformer, the resulting structure (Figure S7d of the Supporting Information) is destabilized by 7.9 kcal/mol. This points to the importance of the hydrogen bond stabilizing interactions between the hydrogen located on nitrogen 1 of the guanine and the nitrogen of the TAP ligand in the most stable conformer (Figure S7c of the Supporting Information).

DOI: 10.1021/acs.jpcb.5b00197
J. Phys. Chem. B 2015, 119, 4488−4500

Table 2. Characteristics of the First Three Calculated Excited States[a]

	$[Ru(TAP)_3]^{2+}$		PA		PA.H$^+$	
ES	λ (nm) (osc)	type	λ (nm) (osc)	type	λ (nm) (osc)	type
1	438 (0.001)	MLCT	505 (0.077)	LLCT	437 (0.0037)	MLCT
2	436 (0)	MLCT	492 (0.040)	ILCT	433 (0.0004)	MLCT/LLCT
3	436 (0)	MLCT	483 (0.008)	LLCT	431 (0.0002)	MLCT/LLCT

[a]Energy (in nanometers), oscillator strength (in parentheses), and description of the first three calculated excited states for $[Ru(TAP)_3]^{2+}$, **PA**, and **PA.H**$^+$ (B3LYP using water as solvent). For the **PA.H**$^+$, the contribution of LLCT is extremely weak.

After determination of the protonated structure, TD-DFT calculations were conducted on the **PA**, **PA.H**$^+$, as well as on the reference $[Ru(TAP)_3]^{2+}$ complex in water. Interestingly, as shown in Figure S8 (panels a−c) of the Supporting Information, a very good match is obtained between the experimental and calculated absorption spectra for the three species. A bathochromically shifted absorption feature near 500 nm is clearly present for the calculated nonprotonated form of **PA** (Figure S8b of the Supporting Information) as observed experimentally at pH 8.0, whereas it is not present for **PA.H**$^+$ (Figure S8c of the Supporting Information). This finding is thus in full agreement with the change of absorption observed as a function of pH (Figure 2a and Figure S2 of the Supporting Information).

If we consider the localization of the different orbitals involved in the electronic transitions (Table S1 of the Supporting Information) for the three species $[Ru(TAP)_3]^{2+}$, **PA**, and **PA.H**$^+$, and more particularly the HOMO−LUMO transitions (Table 2 and Figure S8 of the Supporting Information), the following conclusions can be drawn. For the reference complex $[Ru(TAP)_3]^{2+}$, obviously the most bathochromic transitions correspond to MLCT transitions (Figure S8d of the Supporting Information and Table 2). For the basic form of **PA**, the lowest energetic transitions have a ligand-to-ligand charge transfer (LLCT) character, with an electron shift from guanine to the TAP ligands, and feature as well an intraligand CT contribution (in TAP(GMP), ILCT, Figure S8e of the Supporting Information and Table 2). These CT transitions are responsible for the appearance of the bathochromic shoulder at 500 nm at pH 8. In contrast, for the protonated **PA.H**$^+$ species, the absorption band, more energetic than the CT transitions at pH 8, corresponds to a mixture of MLCT transitions (Figure S8 (panels f1−f3) of the Supporting Information and Table 2), with an extremely weak contribution of LLCT. Thus, mainly MLCT transitions from Ru toward TAPGH$^+$ and TAP ligands are responsible for the most bathochromic absorption. These results are important for the assignment of the transient absorptions below.

On the basis of the relative energies of the HOMO and LUMO levels of the three species (Table 2 and Table S1 of the Supporting Information), conclusions concerning the electrochemical behavior described above can also be drawn. The oxidation and reduction potentials in Table 1 would belong more probably to the protonated **PA.H**$^+$ species. Indeed the HOMO level of **PA.H**$^+$ is close to that centered on the Ru^{II} of $[Ru(TAP)_3]^{2+}$, in agreement with the small difference in the oxidation potentials of the reference complex and protonated **PA**, in contrast to a larger difference between the HOMO levels of nonprotonated **PA** and $[Ru(TAP)_3]^{2+}$. The second oxidation wave could probably be attributed to oxidation of the GMPH$^+$ substituent. Moreover, the LUMO level of **PA.H**$^+$ is more stabilized than that for $[Ru(TAP)_3]^{2+}$ and for **PA**, in agreement with the less negative reduction potential of the first reduction wave measured for the photoadduct. Arguments are thus in favor of the presence of **PA** in its protonated form in the MeCN solution during the electrochemical experiments.

3.4. Resonance Raman Spectroscopy of PA. In order to confirm experimentally the participation of LLCT and/or ILCT transitions to the bathochromic electronic absorption of nonprotonated **PA** at pH 8, resonance Raman (rR) spectra were recorded at 532 nm, thus in the absorption shoulder of nonprotonated **PA** (Figure 2a, blue curve). Moreover, rR measurements were also performed at pH 7.4 and 5.9. For comparison purposes, the rR spectrum of $[Ru(TAP)_3]^{2+}$ at the same 532 nm laser wavelength was recorded as well as the Raman spectrum of GMP (at 473 nm) (Figure S9 of the Supporting Information and Table 3).

Table 3. Vibration Frequencies in Resonance Raman[a]

PA (pH 8)	$[Ru(TAP)_3]^{2+}$	GMP
rR (freq/cm^{-1})	rR (freq/cm^{-1})	Raman (freq/cm^{-1})
927		
960		
1022[b]	1015	
1071[b]		1075
1136		
1205[b] (1184 sh)		1221
1253		
1269[b]		1267
		1313
1355		
1395[b] (1383 sh)		1390
1461[b] (1441 sh)[b]	1420	1481
1550		

[a]Comparison of the vibration frequencies in resonance Raman (laser wavelength 532 nm) for **PA** at pH 8.0 and $[Ru(TAP)_3]^{2+}$ and in Raman spectroscopy (laser wavelength at 473 nm) for GMP. [b]Frequencies similar to those of GMP and $[Ru(TAP)_3]^{2+}$

It is first observed that for the same concentration, the intensities of the frequency signals of the **PA** decrease with decreasing the pH from 8.0 to 5.9 (Figure S9a of the Supporting Information), which is in agreement with the blue shift of the 500 nm absorption shoulder by protonation of **PA**.

A second observation (Table 3) is that some rR frequencies of **PA** seem to be characteristic of the GMP substitution in **PA**, such as 1071, 1269, and 1395 cm^{-1} as compared to 1075, 1267, and 1390 cm^{-1}, respectively, for the Raman frequencies of GMP. This confirms thus the participation of the LLCT/ILCT transitions.

Other comparisons of the rR spectra of **PA** with those of the reference compounds are less obvious. Indeed the rR vibrations of TAP in $[Ru(TAP)_3]^{2+}$ at 532 nm are extremely weak (Figure S9 of the Supporting Information), since this wavelength is in the absorption tail of the MLCT transition Ru-TAP, which

DOI: 10.1021/acs.jpcb.5b00197
J. Phys. Chem. B 2015, 119, 4488−4500

does not facilitate the comparison. Moreover, the **PA** could exhibit some differences in the TAP vibrations due to a change of symmetry in the molecule and a change of chromophore (i.e., MLCT and LLCT/ILCT transitions). Taking this into account, in the rR of **PA**, the 1022 and 1441 cm^{-1} signals could be attributed to TAP ligand frequencies that appear at 1015 and 1420 cm^{-1}, respectively, in the rR spectrum of $[Ru(TAP)_3]^{2+}$. In contrast, the 1205 and 1461 cm^{-1} signals in **PA** could be assigned to the guanine, the frequency of which appears at 1221 and 1481 cm^{-1}, respectively, in the Raman spectrum of GMP.

In conclusion, the TD-DFT calculations and rR spectroscopy clearly support the data of absorption and voltammetry. As both the protonated and nonprotonated forms of **PA** are nonluminescent, both excited species have been further studied in view of explaining the absence of luminescence and the origin of formation of biphoto-adducts in the presence of GMP (addition of a second GMP moiety to the **PA**). Therefore, both forms of the photoadduct, **PA** and **PA.H**$^+$, were examined by laser-induced time-resolved spectroscopy in order to highlight their similar or different behaviors.

3.5. Ultrafast Spectroscopy of the Reference Complex $[Ru(TAP)_3]^{2+}$. Before studying by ultrafast spectroscopy, the **PA**/**PA.H**$^+$, the reference complex (i.e., $[Ru(TAP)_3]^{2+}$) was examined. The photophysics of $[Ru(TAP)_3]^{2+}$ has been well-documented in the literature,[11,41] at least in the nanoseconds time-domain. This complex emits in water and in MeCN from the ^{3}MLCT state with a lifetime under an argon atmosphere of 223 and 68 ns, respectively.[41] Although several works in ultrafast spectroscopy have been conducted with $[Ru(bpy)_3]^{2+}$,[42−47] no studies have ever been performed until now in the pico- and femto-second time-domain for the $[Ru(TAP)_3]^{2+}$ complex. These data are needed for a comparison with the behavior of **PA** and **PA.H**$^+$ in the same timescale. The ultrafast transient absorption spectra from excitation of $[Ru(TAP)_3]^{2+}$ by a 100 fs pulse at 400 nm in buffered aqueous solution are shown in Figure 4a.

Within the excitation pulse, a transient spectrum with three different bands appears. A negative band in the 375−500 nm region with a maximum at 440 nm corresponds to the depopulation of the ground state, whereas two positive bands, one below 375 nm and another one above 550 nm, are attributed to the formation of excited states. Within 1 ns, the UV positive band with a maximum at 340 nm decreases by about 70% (Figure 4a and Table 4), and its decay is characterized by a short minor time constant of a few picoseconds and a major long one of several hundred picoseconds (Table 4). During the first step, the maximum of the band at 340 nm is slightly blue-shifted, which is assigned to intramolecular vibrational relaxation (IVR) and vibrational relaxation (VR) assisted by the solvent from vibrationally hot excited states. The depopulation band (at 440 nm) and weak positive band above 550 nm are characterized by the same time constant values as observed for the 340 nm UV-band within the experimental error (Table 4). This is confirmed by a global decay analysis (Figure S10 of the Supporting Information). Two time constants are thus retrieved from a single wavelength fitting, 2.2 ± 0.8 ps (IVR/VR) and 633 ± 150 ps, respectively (at 340 nm for example, Table 4). The error for the longer component (633 ps) is intrinsic to the experiments. By single photon counting experiments, a value of about 740 ± 50 ps was determined (Figure S11 of the Supporting Information); taking the errors into consideration, this value is in relatively good agreement with the value found in absorption.

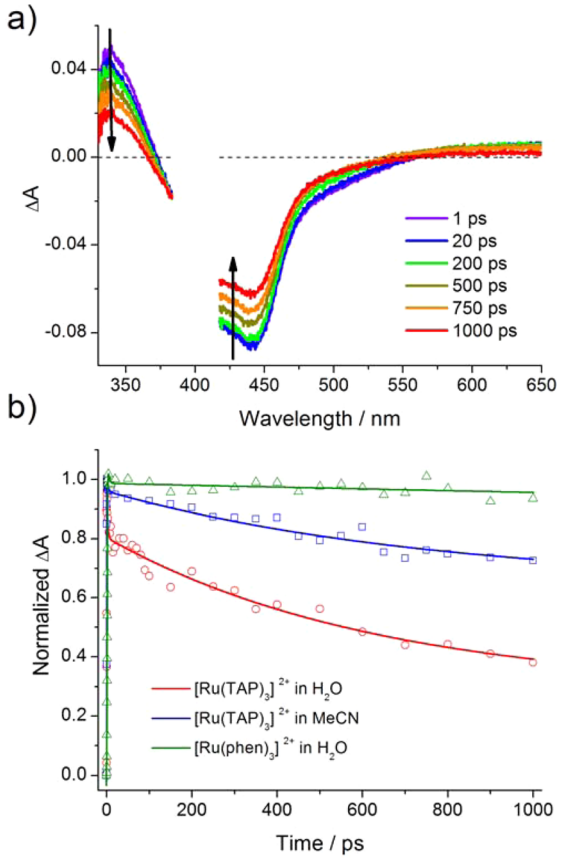

Figure 4. (a) Ultrafast transient absorption spectra of $[Ru(TAP)_3]^{2+}$ in H_2O (0.1 M Tris buffer pH 7). (b) Normalized transient absorption time profiles for $[Ru(TAP)_3]^{2+}$ in H_2O (at 340 nm, red), $[Ru(TAP)_3]^{2+}$ in MeCN (at 340 nm, blue), and $[Ru(phen)_3]^{2+}$ in H_2O (at 330 nm, green).

This several hundred picoseconds decay was unexpected. It has to be underlined that, in contrast to the classical bpy ligand, the TAP ligand possesses two additional nonchelating nitrogen atoms that might be involved in H-bond formation with water and buffer molecules.[38] Moreover, the basicity of the TAP ligand is enhanced in the ^{3}MLCT excited state of the complex, in which one TAP ligand bears a negative charge.[38] The transient which decays in about 700 ps could thus be attributed to the excited ^{3}MLCT state forming H-bonds with water/buffer molecules due to the increased basicity upon excitation. This process is accompanied by a decay to the ground state (see depopulation band recovery in Figure 4 and Table 4), involving vibronic coupling via the hydrogen bond (internal conversion, IC)[48,49] so that more or less 60% of the initially laser produced excited states relax to the ground state. The 40% remaining H-bonded excited species decay afterward in the nanosecond time domain to the ground state in 223 ns. This is in full agreement with previous data,[38] showing that the luminescence lifetimes of $[Ru(TAP)_3]^{2+}$ measured in the nanoseconds timescale depend on the buffer; the emission is quenched differently with a static quenching contribution by different buffers for a same pH value. We tried to confirm further this hypothesis by conducting the same measurements with $[Ru(TAP)_3]^{2+}$ in acetonitrile and with $[Ru(phen)_3]^{2+}$ in water, since this latter complex should not be able to form H bonds because the phenanthroline ligand has no free nonchelating nitrogen atoms. As it is observed in Figure 4b, the long decay component

DOI: 10.1021/acs.jpcb.5b00197
J. Phys. Chem. B 2015, 119, 4488−4500

Table 4. Time Constants[a]

complex	solvent[b]	single wavelength fitting	
		λ (nm)	τ (ps) (amp)[c]
$[Ru(TAP)_3]^{2+}$	H_2O	340	2.2 ± 0.8 (0.0089)
			633 ± 150 (0.0254)
			>1000 (0.0147)[d]
		440	2.9 ± 0.8 (−0.0032)
			735 ± 150 (−0.0521)
			>1000 (−0.0373)[d]
PA.H$^+$	H_2O	480	1.6 ± 0.3 (0.0036)
			12.8 ± 3 (−0.0041)
			159 ± 25 (−0.0216)
			>1000 (0.0322)
	D_2O	480	1.5 ± 0.3 (0.0058)
			20.4 ± 6 (−0.0081)
			328 ± 40 (−0.0282)
			>1000 (0.0401)
PA	H_2O	550	3.0 ± 0.4 (0.0041)
			222 ± 40 (0.0027)
			>1000 (0.0135)
	D_2O	550	3.2 ± 0.6 (0.0028)
			258 ± 40 (0.0028)
			>1000 (0.0123)

[a]Time constants obtained by fitting the kinetic traces recorded in femtosecond transient absorption experiments for $[Ru(TAP)_3]^{2+}$, **PA**, and **PA.H**$^+$. [b]Samples were dissolved in aqueous TRIS buffered solutions with pH and pD 7.0 for $[Ru(TAP)_3]^{2+}$, 5.9 for **PA.H**$^+$ and 8.0 for **PA**. [c]Estimated error for the amplitudes is ±10%. See the Supporting Information for all the global analyses. [d]The long component was fixed during the fitting procedure to the value of 223 ns, which was obtained from nanosecond experiment.

(around 633 ps) for $[Ru(TAP)_3]^{2+}$ in buffered solution is quasi absent in MeCN and does not exist for $[Ru(phen)_3]^{2+}$ in water. In conclusion, although an extremely weak decay contribution is still detectable in MeCN (probably due to remaining water in this solvent), the fact that (i) the 700 ps decay is absent for $[Ru(phen)_3]^{2+}$, (ii) it has almost disappeared in MeCN for $^3[Ru(TAP)_3]^{2+}$, and (iii) the luminescence of the produced species after the 700 ps process depends on the buffer (concentration and type of buffer),[38] confirms the possible origin of this transient as H-bonded excited $^3[Ru(TAP)_3]^{2+}$. Scheme 1 could be proposed for the dynamic processes for $[Ru(TAP)_3]^{2+}$ in aqueous buffered solution.

3.6. Ultrafast Spectroscopy of the Photoadduct. The decay analysis for the excited **PA** is even more challenging. Indeed, taking into account the pH influence on the absorption spectrum, at least two species **PA** and **PA.H**$^+$ can be present in the ground state. Of course, the pH medium can be adjusted, but the pH window is rather limited for experimental reasons. As mentioned above, at high pH values (pH > 8) dechelation of the ligand from the metal center does occur. Moreover, at pH < 5, a protonation of TAP ligands takes place in the excited state.[38] Therefore, the analyses using a 400 nm pulsed excitation were performed at pHs 5.9 and 8.0.[50]

3.6.a. Transient Absorption at pH 5.9. Similarly to the $[Ru(TAP)_3]^{2+}$ case, the transient absorption spectrum formed immediately after femtosecond excitation (spectrum at 0.6 ps, Figure 5a) is also characterized by three bands, two positive

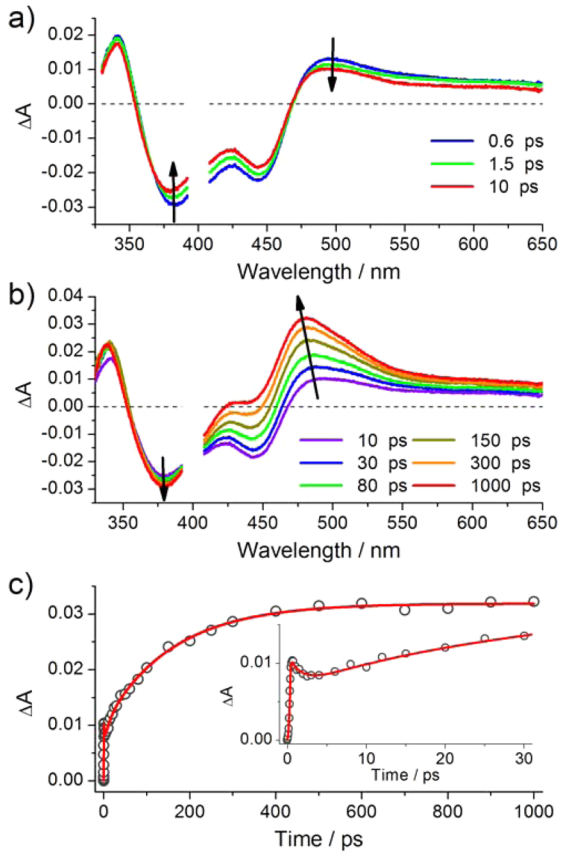

Figure 5. Ultrafast transient absorption spectra of **PA.H**$^+$ at pH 5.9 recorded (a) from 0.6 to 10 ps and (b) from 10 ps to 1 ns after the pulse. (c) Evolution of the transient absorption signal at 480 nm up to 1 ns (inset: from 0 to 30 ps). Fitting according to a multiexponential function with time constants of 1.6 ± 0.3, 12.8 ± 3, and 159 ± 25 ps.

Scheme 1. Dynamic Processes for Excited $[Ru(TAP)_3]^{2+}$; "Hot" for Vibrationally Excited States

$$[Ru^{II}(TAP)_3]^{2+} \xrightarrow{h\nu} {}^1[Ru^{III}(TAP)_2(TAP^{\bullet-})]^{2+*} \quad (1)$$

$${}^1[Ru^{III}(TAP)_2(TAP^{\bullet-})]^{2+*} \xrightarrow{ISC} \text{hot } {}^3[Ru^{III}(TAP)_2(TAP^{\bullet-})]^{2+*} \quad (2)$$

$$\text{hot } {}^3[Ru^{III}(TAP)_2(TAP^{\bullet-})]^{2+*} \xrightarrow[<5\text{ ps}]{VR/IVR} {}^3[Ru^{III}(TAP)_2(TAP^{\bullet-})]^{2+*} \quad (3)$$

$${}^3[Ru^{III}(TAP)_2(TAP^{\bullet-})]^{2+*} \xrightarrow[\sim 700\text{ ps}]{\text{H-bond}} \begin{cases} [Ru^{II}(TAP)_3]^{2+} \\ \text{H-bonded } {}^3[Ru^{III}(TAP)_2(TAP^{\bullet-})]^{2+*} \end{cases} \quad (4)$$

$$\text{H-bonded } {}^3[Ru^{III}(TAP)_2(TAP^{\bullet-})]^{2+*} \xrightarrow[223\text{ ns}]{} \text{H-bonded } [Ru^{II}(TAP)_3]^{2+} \quad (5)$$

DOI: 10.1021/acs.jpcb.5b00197
J. Phys. Chem. B 2015, 119, 4488−4500

Scheme 2. Dynamic Processes for the Excited PA.H$^+$

$$[Ru^{II}(TAP)_2(TAP(GH)^+)]^{3+} \xrightarrow[<5\ ps]{h\nu \text{ and ISC/VR/IVR}} {}^3[Ru^{III}(TAP)(TAP^{\bullet-})(TAP(GH)^+)]^{3+*} \xrightarrow{IC} [Ru^{II}(TAP)_2(TAP(GH)^+)]^{3+} \quad (6)$$

$$[Ru^{II}(TAP)_2(TAP(GH)^+)]^{3+} \xrightarrow[<5\ ps]{h\nu \text{ and ISC/VR/IVR}} {}^3[Ru^{III}(TAP)_2(TAP^{\bullet-}(GH)^+)]^{3+*} \xrightarrow{IC} [Ru^{II}(TAP)_2(TAP(GH)^+)]^{3+} \quad (6')$$

$${}^3[Ru^{III}(TAP)(TAP^{\bullet-})(TAP(GH)^+)]^{3+*} \xrightarrow[159\ ps]{PT} {}^3[Ru^{III}(TAP)(TAPH^{\bullet})(TAP(G))]^{3+*} \quad (7)$$

$${}^3[Ru^{III}(TAP)_2(TAP^{\bullet-}(GH)^+)]^{3+*} \xrightarrow[159\ ps]{PT} {}^3[Ru^{III}(TAP)_2(TAPH^{\bullet}(G))]^{3+*} \quad (7')$$

$${}^3[Ru^{III}(TAP)(TAPH^{\bullet})(TAP(G))]^{3+*} \xrightarrow{PCET} [Ru^{II}(TAP)(TAPH^{\bullet})(TAP(G(-H))^{\bullet})]^{2+} + H^+ \quad (8)$$

$${}^3[Ru^{III}(TAP)_2(TAPH^{\bullet}(G))]^{3+*} \xrightarrow{PCET} [Ru^{II}(TAP)_2(TAPH^{\bullet}(G(-H))^{\bullet})]^{2+} + H^+ \quad (8')$$

bands for the formation of photoexcited states and the negative depopulation band of the ground state. However, instead of a very weak positive absorption at wavelengths >550 nm observed for $[Ru(TAP)_3]^{2+}$, the visible positive band for **PA.H**$^+$ starts from 475 nm with a maximum at 490 nm and a broad shoulder from 550 nm. Such a difference is assigned to the presence of the G unit in the photoadduct structure. Within a few picoseconds, a short decay of the entire spectrum is observed and attributed to the combination of cooling processes (IVR and VR in comparison with $[Ru(TAP)_3]^{2+}$) and relaxation to the ground state (IC) because the depopulation band is decreasing (Figure 5a and Table 4). Afterward, while the positive absorption band around 340 nm and depopulation band around 375 nm remain quasi constant, the band centered at 490 nm increases in a few hundred picoseconds. Moreover, this increase is accompanied by a blue shift of the maximum to a value of 480 nm, and at the same time, by a decrease of the depopulation band at around 450 nm due to a strong overlapping with the increasing of the 480−490 nm band (Figure 5b). The final spectrum at 1 ns remains unchanged and is similar to the one obtained by nanosecond transient absorption experiments (vide infra). The single wavelength fitting at 480 nm gives three time constants, one decay (1.6 ps) and two growing ones, 12.8 and 159 ps (Figure 5c and Table 4). As it can be seen in the decay associated spectra obtained by global analysis (Figure S12 of the Supporting Information), the shorter growing time constant has a minor contribution, and its maximum is shifted in comparison to the major long decay. Such biexponential fit is characteristic of a growing band concomitantly with a shift of its maximum, and only the main contribution time constant will be taken into account for this step of growing absorption.[51] Since at pH 5.9, the excited state should mainly correspond to the protonated excited **PA.H**$^+$, after relaxation of this state, some proton transfers could be imagined for the next steps. Therefore, we performed the same time-resolved experiments in heavy water D_2O at pD 5.9 in order to test whether the transient exhibit an isotopic effect. This is indeed the case since the time constant increases from 159 to 328 ps (Figures S13 and S14 of the Supporting Information and Table 4). The initial protonated excited state **PA.H**$^{+}$* is thus transformed into other species involving proton transfer(s) and giving rise to a continuous absorption band shift during continuous dynamic processes within a 1 ns time-window without repopulation of the ground state of the starting complex.

On the basis of the TD-DFT calculations (Table 2, Table S1 and Figure S8 of the Supporting Information), mainly two different MLCT electronic transitions are involved in the visible absorption of **PA.H**$^+$. As is generally accepted for the Ru complexes that the MLCT character in absorption is kept in emission, we could infer from these theoretical data that the lowest relaxed protonated excited states should correspond to ^{3}MLCT states. Therefore, following the cooling processes and some relaxation to the ground state in 1.6 ps (in H_2O), depending on the localization of the excited electron on one or the other ligand in the excited protonated ^{3}MLCT states, two possible states could be produced, one with the electron on a TAP ligand (Scheme 2, eq 6) and another with the electron on the TAP bearing the GMP unit (Scheme 2, eq 6′).

The following reaction steps after population and relaxation of the ^{3}MLCT excited states could be proposed (see Scheme 2). (i) In eq 6 or 6′, the TAP$^{\bullet-}$ motif of the excited state is rather basic (see pK_a* of the excited Ru-TAP complexes).[38] Therefore, due to this sudden increase of local basicity, a proton transfer (PT) could take place from the protonated guanine group GH$^+$ to the TAP$^{\bullet-}$ motif (eq 7 or 7′). (ii) Thanks to this deprotonation in the excited state (thus thanks to the acid−base reaction in the ^{3}MLCT excited states), the deprotonated G substituent would then behave as an electron donor versus the oxidizing Ru^{III} center of the ^{3}MLCT states. This would result into an intramolecular electron transfer from G to Ru^{III} (eqs 8 and 8′) most probably accompanied by deprotonation of the G radical cation (PCET, see also below). These processes would thus be responsible for the luminescence quenching of the ^{3}MLCT excited states.

The reactions 7−7′ to 8−8′ would constitute continuous dynamic processes taking place in 159 ps (328 ps in D_2O) with a continuous blue shift of absorption without restoration of the starting material. At the end of these transformations (1 ns) long-lived radical species like those formed in eqs 8−8′ and observed in the nanosecond time domain (see below) would be formed.

In favor of these hypotheses, the following independent data can be cited. (i) The resemblance between the transient spectrum in Figure 5b with the one obtained in the past for the "classical" intermolecular photoelectron transfer between excited $[Ru(TAP)_3]^{2+}$ and free GMP as electron donor (see Introduction) is striking (Figure S15a of the Supporting Information).[52] Of course, in this latter case of intermolecular reaction, the electron transfer quenching is slow because it is diffusion limited ($k_{ET} > 10^9\ s^{-1}$). Importantly, in that case, the transients in the hundred microseconds time domain had been unambiguously assigned to the reduced protonated complex and deprotonated radical cation of the GMP guanine (thus two solvated radicals, Figure S15b of the Supporting Information).

These radical intermediates have a strong resemblance with the proposed biradical produced in eqs 8−8′, except that in this case the processes are intramolecular. (ii) In another case, the

DOI: 10.1021/acs.jpcb.5b00197
J. Phys. Chem. B 2015, 119, 4488−4500

Ru-TAP complex intercalated in a DNA helix where the diffusion step is absent, the characteristic time constant for the electron transfer from a DNA guanine base to the excited complex corresponds to 480 ps.[27] Because of an isotopic effect, this process was proposed to be kinetically coupled to deprotonation of the guanine radical cation. Therefore, in the present case, the same kinetically coupled process is considered in eqs 8−8′. (iii) The triggering event for the continuous reactions from 6−6′ to 8−8′ with luminescence quenching would thus be the deprotonation of the GH^+ substituent of the excited **PA.H**$^+$. Indeed, a direct electron transfer (ET) from GH^+ would not be possible because an ET from a GMP guanine to the excited complex is already very weakly exergonic (ΔG^0 = −0.07 eV),[20] thus an ET process from a protonated guanine would have still a lower probability to occur.

In conclusion, by population of the excited ^{3}MLCT states of **PA.H**$^+$, an acid−base reaction would take place in the excited states, triggered by the basicity of the produced $TAP^{\bullet-}$ motif. This leads to a continuous transformation with quenching of the excited states with a time constant of 159 ps (328 ps in D_2O) and with formation of the proposed ground state long-lived biradical species (eqs 8−8′). Moreover, these continuous processes would include two intracomplex proton transfers (or transfer via water molecules) in agreement with the isotopic effect. This whole scheme would thus explain the absence of luminescence of the photoadduct at pH 5.9.

3.6.b. Transient Absorption at pH 8.0. At pH 8.0, mainly the deprotonated form of the photoadduct should be present.[50] Since there is a bathochromic shoulder around 500 nm in the electronic absorption spectrum, excitation wavelengths in this region could be used. However, the 400 nm excitation was preferred because of a higher molar absorption coefficient at that wavelength and because excitation around 500 nm prevents transient absorption kinetic analyses at 480 nm, which is a key wavelength for the transients detection.

Figure 6 (panels a and b) shows the transient absorption spectra recorded at pH 8.0 as a function of time. The spectra and dynamic behavior are different from those at pH 5.9. Whereas at pH 5.9 a strong absorption band appears at 490 nm within excitation and increases in 159 ps, only a broad band at wavelengths >525 nm with a maximum around 550 nm is observed at pH 8.0. This band disappears in two steps, a first one in a few picoseconds and a second one in a few hundred picoseconds concomitantly with the decay of the band at 350 nm and the depopulation recovery. After 1 ns, a very weak remaining absorption is still observable with a slight maximum at 480 nm.

On the basis of the pK_a of the **PA** and the above data for the protonated photoadduct, it is probable that this remaining spectrum at pH 8.0 could be assigned to the **PA.H**$^+$ photoproducts. Indeed, some participation (less than 10%) of the protonated species can still be excited at pH 8.0. Kinetic analyses (Figure 6c, Table 4 and Figure S17 of the Supporting Information for D_2O) at 550 nm as well as global analysis (Figure S16 and Figure S18 of the Supporting Information) give two time constants of 3.0 and 222 ps, which are almost nonsensitive to D_2O (3.2 and 258 ps). The first time constant is assigned to vibrational relaxation and internal conversion to ground state as depopulation recovery is observed. On the basis of the TD-DFT calculations (Table 2 and Table S1 and Figure S8 (panels b and e) of the Supporting Information), the few hundred picoseconds decay (222 ps) is assigned to relaxation of

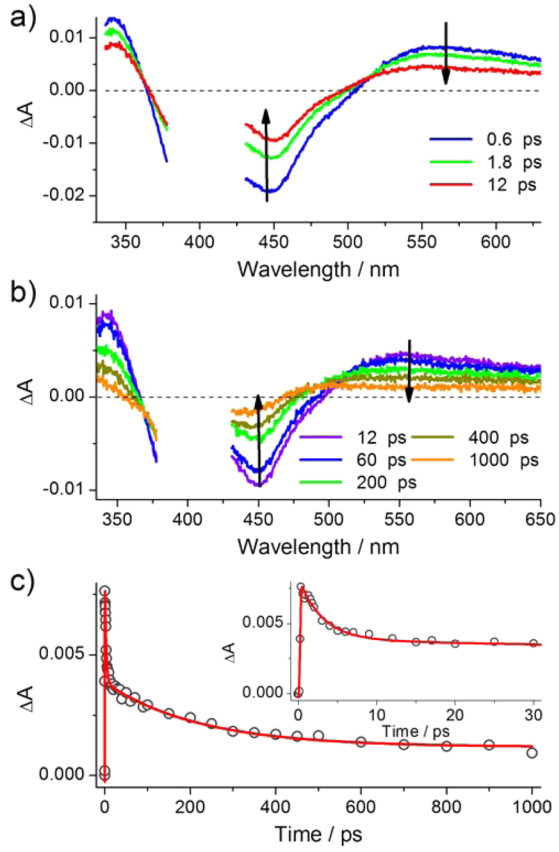

Figure 6. Ultrafast transient absorption spectra of **PA** at pH 8.0 recorded (a) from 0.6 to 12 ps and (b) from 12 ps to 1 ns after the pulse. (c) Evolution of the transient absorption signal at 550 nm up to 1 ns (inset: from 0 to 30 ps). Fitting according to a multiexponential function with time constants of 3.0 ± 0.4 ps and 222 ± 40 ps.

the lowest CT excited states (i.e., LLCT and/or ILCT excited states).

3.7. Nano- and Microsecond Time Resolved Spectroscopy of the Photoadduct at pH 5.9 and 8.0. According to the conclusions in ultrafast spectroscopy, the process of 159 ps (328 ps in D_2O) at pH 5.9, responsible for the quenching of the excited states, would give rise to biradical species, $[Ru^{II}(TAP)(TAPH^{\bullet})(TAP(G(-H))^{\bullet})]^{2+}$ and $[Ru^{II}(TAP)_2(TAPH^{\bullet}(G(-H))^{\bullet})]^{2+}$ (eqs 8−8′). In order to investigate the slower processes characterizing the reactivity of these species, nanosecond transient absorption measurements have also been carried out.

At pH 5.9 with **PA.H**$^+$, a very long and weak transient is observed as a positive signal at 480 nm and depletion around 400 nm, from 10 ns until a few microseconds (Figure S19 of the Supporting Information).[53]

The spectra are similar to those of Figure 5b, except the presence of a very weak negative signal with a maximum around 625 nm, attributed to emission of contaminating $[Ru(TAP)_3]^{2+}$.[36] These long-lived microseconds radical species could disappear by different possible inter- and/or intramolecular reactions according to complicated kinetics. As noted from the remaining permanent absorption, the reactions of these radicals lead to final stable products (black curve in Figure 7). Interestingly, these long-lived species disappear more rapidly in the presence of added 10 mM GMP (red curve in Figure 7). Because these radical species are the only long-lived transients at pH 5.9 that are able to react with free GMP, it is

DOI: 10.1021/acs.jpcb.5b00197
J. Phys. Chem. B 2015, 119, 4488−4500

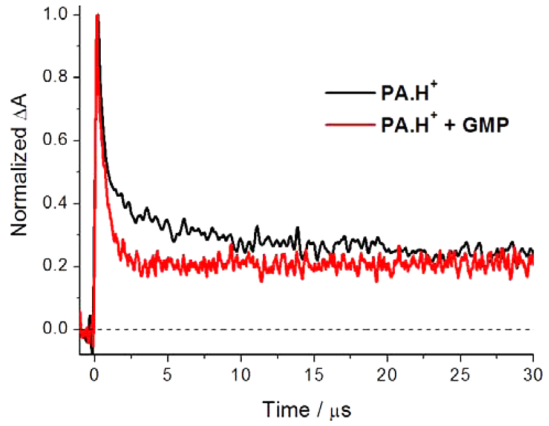

Figure 7. Normalized nanosecond transient absorption signal at 500 nm of the **PA.H**$^+$ at pH 5.9 recorded in the absence (black) and in the presence (red) of GMP 10 mM.

proposed that they would be the origin of formation of the biphoto-adducts. Independent results corroborate this hypothesis; as mentioned above, two types of biphoto-adduct have been detected by mass spectroscopy analyses from solutions of **PA** illuminated at pH 5.9, one with two guanine units covalently attached to the complex via two different TAP ligands and one where the two guanine moieties are on the same TAP ligand (Figure 3 and Figure S5 of the Supporting Information). Thus, this would mean that species like those in eqs 8−8′ (i.e., $[Ru^{II}(TAP)(TAPH^{\bullet})(TAP(G(-H))^{\bullet})]^{2+}$ and $[Ru^{II}(TAP)_2(TAPH^{\bullet}(G(-H))^{\bullet})]^{2+}$) could be the reactive intermediates which react with GMP to produce irreversible biphoto-adducts from the monophoto-adduct **PA.H**$^+$.

In contrast, at pH 8.0, from the nanosecond to the microsecond timescale, no transient can be detected. This is in agreement with the fact that the nonprotonated **PA** has other types of lower excited states (i.e., LLCT/ILCT states), which do not lead to intramolecular proton and electron transfer processes but simply decay to the ground state.

4. CONCLUSIONS

Thanks to a combination of different experimental and theoretical approaches, we succeeded in getting a deep insight in the photophysical processes underlying the behaviors of the monophoto-adduct **PA** formed between $[Ru(TAP)_3]^{2+}$ and a guanine base (Figure 1). The fact that the pK_a value of this **PA** is close to 7 is physiologically important. Indeed, if the local pH would be a bit lower or higher than 7, it will have important consequences on the biadducts formation with GMP or cross-linking with G-containing DNA as mentioned in the introduction. A pH < 6 is essential for producing biadducts.[28,54] The different results of this work demonstrate this very clearly. Thus, the biadducts can be detected by mass spectrometry after irradiation at pH 5.9 and not at pH 8.0. Moreover, it can be concluded that these pH conditions for the **PA** photoreaction can also be fully explained by the **PA** photophysical scheme, which depends on the pH value.

At pH > 8, the nonprotonated **PA** has lowest excited states corresponding to LLCT/ILCT states that control their deactivation to the ground state. These excited states do not lead to radicals that are reactive versus GMP and thus no biadduct is formed. In contrast at pH < 6, **PA.H**$^+$ is present. In that case, after the excitation, MLCT excited states are populated. These states give rise to continuous processes in 159 ps triggered by the enhanced basicity of the $TAP^{\bullet-}$ motif in the excited MLCT states of **PA.H**$^+$. These processes occurring inside the photoadduct explain not only the absence of emission but also the reactivity versus GMP with production of biadducts. It is interesting to note that in agreement with the population of two types of MLCT excited states, based on the results of the TD-DFT study, two different biadducts are produced.

In conclusion, this **PA** study explains not only the photoreactivity of the Ru-TAP complexes versus DNA but also it constitutes to some extend a model study for electron and proton transfer with Ru-TAP complexes and DNA.

■ ASSOCIATED CONTENT

Supporting Information

Steady state emission and absorption, mass spectrometry, resonance Raman, voltammetry, transient absorption, fluorescence decays, and DFT and TD-DFT calculations. This material is available free of charge via the Internet at http://pubs.acs.org.

■ AUTHOR INFORMATION

Corresponding Authors

*E-mail: michel.sliwa@univ-lille1.fr. Tel: 0033320336353. Fax: 0033320436755.

*E-mail: akirsch@ulb.ac.be. Tel.: 003226503017. Fax: 003226503018.

Author Contributions

$^{\perp}$L.M. and M.R. contributed equally to this study. The manuscript was written through contributions of all authors. All authors have given approval to the final version of the manuscript.

Notes

The authors declare no competing financial interest.

■ ACKNOWLEDGMENTS

L.M. thanks the "Fonds National pour la Recherche Scientifique" (FNRS) in Belgium for a Ph.D. grant. A.K.D. and C.M. are grateful to the FRFC-FNRS for financial support (RuPEP and Ru-BINDER projects). M.S., E.F., and M.R. thank financial support from PICS CNRS-FWO Fund. E.F. thanks Prof. M. Van der Auweraer for discussions and Gang Lu and Prof. H. Uji-I for experimental support. The work in Mons was supported by the European Commission/Région Walonne, the Interuniversity Attraction Pole (IUAP 7/05), and the "Programme d'Excellence de la Région Walonne". P.G. and J.D.W. are grateful to the FRS-FNRS for continuing support.

■ REFERENCES

(1) Durham, B.; Caspar, J. V.; Nagle, J. K.; Meyer, T. J. Photochemistry of Tris(2,2′-bipyridine)ruthenium(2+) Ion. *J. Am. Chem. Soc.* **1982**, *104*, 4803−4810.

(2) Caspar, J. V.; Meyer, T. J. Photochemistry of Tris(2,2′-bipyridine)ruthenium(2+) Ion ($Ru(bpy)_3^{2+}$). Solvent Effects. *J. Am. Chem. Soc.* **1983**, *105*, 5583−5590.

(3) Balzani, V.; Campagna, S. Photochemistry and Photophysics of Coordination Compounds I. In *Topics in Current Chemistry*; Springer: Berlin, 2007; Vol. *280*.

(4) Nazeeruddin, M. K.; Zakeeruddin, S. M.; Lagref, J. J.; Liska, P.; Comte, P.; Barolo, C.; Viscardi, G.; Schenk, K.; Graetzel, M. Stepwise Assembly of Amphiphilic Ruthenium Sensitizers and their Applications in Dye-sensitized Solar Cell. *Coord. Chem. Rev.* **2004**, *248*, 1317−1328.

DOI: 10.1021/acs.jpcb.5b00197
J. Phys. Chem. B 2015, 119, 4488−4500

(5) Puntoriero, F.; Sartorel, A.; Orlandi, M.; La Ganga, G.; Serroni, S.; Bonchio, M.; Scandola, F.; Campagna, S. Photoinduced Water Oxidation Using Dendrimeric Ru(II) Complexes as Photosensitizers. *Coord. Chem. Rev.* **2011**, *255*, 2594−2601.
(6) Concepcion, J. J.; Jurss, J. W.; Brennaman, M. K.; Hoertz, P. G.; Patrocinio, A. O. T.; Murakami Iha, N. Y.; Templeton, J. L.; Meyer, T. J. Making Oxygen with Ruthenium Complexes. *Acc. Chem. Res.* **2009**, *42*, 1954−1965.
(7) Sauvage, J.-P. Transition Metal-complexed Catenanes and Rotaxanes as Molecular Machine Prototypes. *Chem. Commun.* **2005**, 1507−1510.
(8) Raehm, L.; Sauvage, J.-P. Molecular Machines and Motors Based on Transition Metal-Containing Catenanes and Rotaxanes. *Struct. Bonding (Berlin, Ger.)* **2001**, *99*, 55−78.
(9) Lo, K. K.-W. Luminescent Transition Metal Complexes as Biological Labels and Probes. In *Photofunctional Transition Metal Complexes*, Yam, V. W., Ed. Springer: Berlin, 2007; Vol. *123*, pp 205−245.
(10) Gill, M. R.; Thomas, J. A. Ruthenium(ii) Polypyridyl Complexes and DNA-from Structural Probes to Cellular Imaging and Therapeutics. *Chem. Soc. Rev.* **2012**, *41*, 3179−3192.
(11) Marcélis, L.; Vanderlinden, W.; Kirsch-De Mesmaeker, A. Probing DNA Using Metal Complexes. In *Inorganic Chemical Biology*; John Wiley & Sons, Ltd: Chichester, West Sussex, England, 2014; pp 183−213.
(12) Zeglis, B. M.; Pierre, V. C.; Barton, J. K. Metallo-intercalators and Metallo-insertors. *Chem. Commun.* **2007**, 4565−4579.
(13) Hall, J. P.; O'Sullivan, K.; Naseer, A.; Smith, J. A.; Kelly, J. M.; Cardin, C. J. Structure Determination of an Intercalating Ruthenium Dipyridophenazine Complex which Kinks DNA by Semiintercalation of a Tetraazaphenanthrene Ligand. *Proc. Natl. Acad. Sci. U.S.A.* **2011**, *108*, 17610−17614.
(14) Elmes, R. B. P.; Orange, K. N.; Cloonan, S. M.; Williams, D. C.; Gunnlaugsson, T. Luminescent Ruthenium(II) Polypyridyl Functionalized Gold Nanoparticles; Their DNA Binding Abilities and Application As Cellular Imaging Agents. *J. Am. Chem. Soc.* **2011**, *133*, 15862−15865.
(15) Elmes, R. B. P.; Kitchen, J. A.; Williams, D. C.; Gunnlaugsson, T. Pushing the Limit: Synthesis, Photophysical and DNA Binding Studies of a NIR-emitting Ru(ii)-polypyridyl Probe with 'Light Switch' Behaviour. *Dalton Trans.* **2012**, *41*, 6607−6610.
(16) Grant, G. J.; Talbott, N. N.; Bajic, M.; Mehne, L. F.; Holcombe, T. J.; VanDerveer, D. G. Heteroleptic Platinum(II) and Palladium(II) Complexes with Thiacrown and Diimine Ligands. *Polyhedron* **2012**, *31*, 89−97.
(17) Miao, T.-F.; Li, S.; Chen, J.-C.; Wang, N.-L.; Zheng, K.-C. Theoretical Studies on DNA-Photocleavage Efficiencies of Ru(ii) Polypyridyl Complexes. *Dalton Trans.* **2013**, *42*, 2463−2468.
(18) Kia, R.; Scholz, M.; Raithby, P. R.; Techert, S. Homoleptic Tetraazaphenanthrene-Based Copper(I) Complexes: Synthesis, Spectroscopic Characterization, Crystal Structures and Computational Studies. *Inorg. Chim. Acta* **2014**, *423*, 348−357.
(19) Véry, T.; Ambrosek, D.; Otsuka, M.; Gourlaouen, C.; Assfeld, X.; Monari, A.; Daniel, C. Photophysical Properties of Ruthenium(II) Polypyridyl DNA Intercalators: Effects of the Molecular Surroundings Investigated by Theory. *Chem.—Eur. J.* **2014**, *20*, 12901−12909.
(20) Marcélis, L.; Ghesquière, J.; Garnir, K.; Kirsch-De Mesmaeker, A.; Moucheron, C. Photo-oxidizing RuII Complexes and Light: Targeting Biomolecules via Photoadditions. *Coord. Chem. Rev.* **2012**, *256*, 1569−1582.
(21) Ghesquière, J.; Gauthier, N.; De Winter, J.; Gerbaux, P.; Moucheron, C.; Defrancq, E.; Kirsch-De Mesmaeker, A. Photocrosslinking between Peptide−Peptide or Peptide−Oligonucleotide by RuII−TAP Complexes. *Chem.—Eur. J.* **2012**, *18*, 355−364.
(22) Jacquet, L.; Kelly, J. M.; Kirsch-De Mesmaeker, A. Photoadduct between Tris(1,4,5,8-tetraazaphenanthrene)ruthenium(II) and Guanosine Monophosphate: A Model for a New Mode of Covalent Binding of Metal Complexes to DNA. *J. Chem. Soc., Chem. Commun.* **1995**, 913−914.
(23) Jacquet, L.; Davies, R. J. H.; Kirsch-De Mesmaeker, A.; Kelly, J. M. Photoaddition of Ru(tap)2(bpy)2+ to DNA: A New Mode of Covalent Attachment of Metal Complexes to Duplex DNA. *J. Am. Chem. Soc.* **1997**, *119*, 11763−11768.
(24) Marcélis, L.; Moucheron, C.; Kirsch-De Mesmaeker, A. Ru−TAP Complexes and DNA: From Photo-Induced Electron Transfer to Gene Photo-Silencing in Living Cells. *Philos. Trans. R. Soc., A* **2013**, *371*.
(25) Ghizdavu, L.; Pierard, F.; Rickling, S.; Aury, S.; Surin, M.; Beljonne, D.; Lazzaroni, R.; Murat, P.; Defrancq, E.; Moucheron, C.; et al. Oxidizing Ru(II) Complexes as Irreversible and Specific Photo-Cross-Linking Agents of Oligonucleotide Duplexes. *Inorg. Chem.* **2009**, *48*, 10988−10994.
(26) Vanderlinden, W.; Blunt, M.; David, C. C.; Moucheron, C.; Kirsch-De Mesmaeker, A.; De Feyter, S. Mesoscale DNA Structural Changes on Binding and Photoreaction with Ru[(TAP)2PHEHAT]-2+. *J. Am. Chem. Soc.* **2012**, *134*, 10214−10221.
(27) Elias, B.; Creely, C.; Doorley, G. W.; Feeney, M. M.; Moucheron, C.; Kirsch-De Mesmaeker, A.; Dyer, J.; Grills, D. C.; George, M. W.; Matousek, P.; et al. Photooxidation of Guanine by a Ruthenium Dipyridophenazine Complex Intercalated in a Double-Stranded Polynucleotide Monitored Directly by Picosecond Visible and Infrared Transient Absorption Spectroscopy. *Chem.—Eur. J.* **2008**, *14*, 369−375.
(28) Kirsch-De Mesmaeker, A.; Nasielski-Hinkens, R.; Maetens, D.; Pauwels, D.; Nasielski, J. Synthesis and Spectroscopic and Electrochemical Properties of a New Ruthenium Complex: The Tris(1,4,5,8-tetraazaphenanthrene)ruthenium(II) Dication. *Inorg. Chem.* **1984**, *23*, 377−379.
(29) Maus, M.; Rousseau, E.; Cotlet, M.; Schweitzer, G.; Hofkens, J.; Van der Auweraer, M.; De Schryver, F. C.; Krueger, A. New Picosecond Laser System for Easy Tunability over the Whole Ultraviolet/Visible/Near Infrared Wavelength Range Based on Flexible Harmonic Generation and Optical Parametric Oscillation. *Rev. Sci. Instrum.* **2001**, *72*, 36−40.
(30) Sliwa, M.; Mouton, N.; Ruckebusch, C.; Poisson, L.; Idrissi, A.; Aloise, S.; Potier, L.; Dubois, J.; Poizat, O.; Buntinx, G. Investigation of Ultrafast Photoinduced Processes for Salicylidene Aniline in Solution and Gas Phase: Toward a General Photo-dynamical Scheme. *Photochem. Photobiol. Sci.* **2010**, *9*, 661−669.
(31) Stoll, T.; Gennari, M.; Serrano, I.; Fortage, J.; Chauvin, J.; Odobel, F.; Rebarz, M.; Poizat, O.; Sliwa, M.; Deronzier, A.; et al. $[Rh^{III}(dmbpy)_2Cl_2]^+$ as a Highly Efficient Catalyst for Visible-Light-Driven Hydrogen Production in Pure Water: Comparison with Other Rhodium Catalysts. *Chem.—Eur. J.* **2013**, *19*, 782−792.
(32) Frisch, M. J.; Trucks, G. W.; Schlegel, H. B.; Scuseria, G. E.; Robb, M. A.; Cheeseman, J. R.; Scalmani, G.; Barone, V.; Mennucci, B.; Petersson, G. A. et al. *Gaussian 09*, Gaussian, Inc.: Wallingford, CT, 2009.
(33) Jmol: An open-source Java viewer for chemical structures in 3D, available at http://www.jmol.org.
(34) Fernández-Hernández, J. M.; Beltrán, J. I.; Lemaur, V.; Gálvez-López, M.-D.; Chien, C.-H.; Polo, F.; Orselli, E.; Fröhlich, R.; Cornil, J.; De Cola, L. Iridium(III) Emitters Based on 1,4-Disubstituted-1H-1,2,3-triazoles as Cyclometalating Ligand: Synthesis, Characterization, and Electroluminescent Devices. *Inorg. Chem.* **2013**, *52*, 1812−1824.
(35) Blasius, R.; Nierengarten, H.; Luhmer, M.; Constant, J.-F.; Defrancq, E.; Dumy, P.; van Dorsselaer, A.; Moucheron, C.; Kirsch-De Mesmaeker, A. Photoreaction of [Ru(hat)2phen]2+ with Guanosine-5′-Monophosphate and DNA: Formation of New Types of Photoadducts. *Chem.—Eur. J.* **2005**, *11*, 1507−1517.
(36) In some cases, the emission lifetime of this weak remaining luminescence could be measured with a nanosecond pulsed laser. The excited state lifetimes corresponded to those of traces of contaminating $[Ru(TAP)_3]^{2+}$, the presence of which is also detected by a minimum at 625 nm in the transient absorption spectrum (Figure S19 (panels a and b) of the Supporting Information).
(37) Mahler, H. R.; Cordes, E. H. *Biological Chemistry*; Harper and Row: New York, 1967.

DOI: 10.1021/acs.jpcb.5b00197
J. Phys. Chem. B 2015, 119, 4488−4500

(38) Kirsch-De Mesmaeker, A.; Jacquet, L.; Nasielski, J. Ruthenium(II) Complexes of 1,4,5,8-tetraazaphenanthrene (TAP) and 2,2′-bipyridine (bpy). Ground- and Excited-State Basicities of Ru2+(bpy)n(TAP)3-n (n = 0, 1, 2): Their Luminescence Quenching by Organic Buffers. *Inorg. Chem.* **1988**, *27*, 4451−4458.
(39) A pH 8 is the maximum pH value, which can be tested, otherwise the Ru-TAP complexes decompose in the dark.
(40) Jang, Y. H.; Goddard, W. A.; Noyes, K. T.; Sowers, L. C.; Hwang, S.; Chung, D. S. pKa Values of Guanine in Water: Density Functional Theory Calculations Combined with Poisson−Boltzmann Continuum−Solvation Model. *J. Phys. Chem. B* **2003**, *107*, 344−357.
(41) Masschelein, A.; Jacquet, L.; Kirsch-De Mesmaeker, A.; Nasielski, J. Ruthenium Complexes with 1,4,5,8-tetraazaphenanthrene. Unusual Photophysical Behavior of the Tris-homoleptic Compound. *Inorg. Chem.* **1990**, *29*, 855−860.
(42) Curtright, A. E.; McCusker, J. K. Static and Time-Resolved Spectroscopic Studies of Low-Symmetry Ru(II) Polypyridyl Complexes. *J. Phys. Chem. A* **1999**, *103*, 7032−7041.
(43) Bhasikuttan, A. C.; Suzuki, M.; Nakashima, S.; Okada, T. Ultrafast Fluorescence Detection in Tris(2,2′-bipyridine)ruthenium(II) Complex in Solution: Relaxation Dynamics Involving Higher Excited States. *J. Am. Chem. Soc.* **2002**, *124*, 8398−8405.
(44) McCusker, J. K. Femtosecond Absorption Spectroscopy of Transition Metal Charge-Transfer Complexes. *Acc. Chem. Res.* **2003**, *36*, 876−887.
(45) Wallin, S.; Davidsson, J.; Modin, J.; Hammarström, L. Femtosecond Transient Absorption Anisotropy Study on [Ru(bpy)3]2+ and [Ru(bpy)(py)4]2+. Ultrafast Interligand Randomization of the MLCT State. *J. Phys. Chem. A* **2005**, *109*, 4697−4704.
(46) Hoff, D. A.; Silva, R.; Rego, L. G. C. Subpicosecond Dynamics of Metal-to-Ligand Charge-Transfer Excited States in Solvated [Ru(bpy)3]2+ Complexes. *J. Phys. Chem. C* **2011**, *115*, 15617−15626.
(47) Cannizzo, A.; van Mourik, F.; Gawelda, W.; Zgrablic, G.; Bressler, C.; Chergui, M. Broadband Femtosecond Fluorescence Spectroscopy of [Ru(bpy)3]2+. *Angew. Chem., Int. Ed.* **2006**, *45*, 3174−3176.
(48) Biczók, L.; Bérces, T.; Linschitz, H. Quenching Processes in Hydrogen-Bonded Pairs: Interactions of Excited Fluorenone with Alcohols and Phenols. *J. Am. Chem. Soc.* **1997**, *119*, 11071−11077.
(49) Horrocks, D. L. Fluorescence Self-Quenching through Hydrogen Bonding. *J. Chem. Phys.* **1969**, *50*, 4151−4156.
(50) At pH 5.9, there is eight times more **PA.H**$^+$ than **PA**, and at pH 8, there is fifteen times more **PA** than **PA.H**$^+$ respectively.
(51) Debus, B.; Sliwa, M.; Miyasaka, H.; Abe, J.; Ruckebusch, C. Multivariate Curve Resolution: Alternating Least Squares to Cope with Deviations from Data Bilinearity in Ultrafast Time-Resolved Spectroscopy. *Chemom. Intell. Lab. Syst.* **2013**, *128*, 101−110.
(52) Lecomte, J.-P.; Kirsch-De Mesmaeker, A.; Kelly, J. M.; Tossi, A. B.; Görner, H. Photo-Induced Electron Transfer from Nucleotides to Ruthenium-tris-1,4,5,8tetraazaphenanthrene: Model for Photosensitized DNA Oxidation. *Photochem. Photobiol.* **1992**, *55*, 681−689.
(53) From 1 to 10 ns, some back electron−proton transfer process with restoration of the starting material cannot be excluded. On DNA with an intercalating Ru−TAP complex, such a process is on the order of 10 ns.[27]
(54) Let us note, however, that pH values lower than 5 have to be avoided because of the protonation of the TAP ligands in the excited state at these pH values.[28]

DOI: 10.1021/acs.jpcb.5b00197
J. Phys. Chem. B 2015, 119, 4488−4500